Phys. Status Solidi B **248**, No. 11, 2635–2638 (2011) / **DOI** 10.1002/pssb.201100510

physica status solidi b
www.pss-b.com
basic solid state physics

Dominant phonon wavevectors of the 2*D* Raman mode of graphene

Rohit Narula[*,1,2], **Nicola Bonini**[3], **Nicola Marzari**[3], **and Stephanie Reich**[2]

[1] Department of Materials Science and Engineering, Massachusetts Institute of Technology, Cambridge, MA 02139, USA
[2] Fachbereich Physik, Freie Universität Berlin, Arnimallee 14, Berlin 14195, Germany
[3] Department of Materials, University of Oxford, Oxford OX1 3PH, United Kingdom

Received 10 August 2011, revised 28 September 2011, accepted 29 September 2011
Published online 21 October 2011

Keywords dominant electronic transitions, graphene, inner and outer processes, phonon mapping, polarized Raman measurements, Raman spectroscopy, 2*D* Raman mode

* Corresponding author: e-mail rnarula@mit.edu, Phone: +1 617 253 3300, Fax: +1 617 252 1175

We investigate the dominant phonon wavevectors $\boldsymbol{q}^*$ and the associated dominant phonon-assisted electronic transitions implied by the 2*D* Raman mode of graphene by combining *ab initio* calculations with a full two-dimensional integration over the graphene Brillouin zone. We find that $\boldsymbol{q}^*$ are highly anisotropic and rotate with the polarizer:analyzer condition, providing access to the entire angular extent around $\boldsymbol{K}$. The resonant electronic transitions do not lie along the $\boldsymbol{K}-\boldsymbol{M}-\boldsymbol{K}'$ line and can be transformed from being apparently "inner" to "outer" with the addition of a reciprocal lattice vector, showing that both are equivalent. We thus invalidate the notion of "inner" and "outer" processes completely.

1 Introduction Raman spectroscopy is a quick and non-destructive means of probing the phonons of graphene [1] and its allotropes [2]. It is routinely used to determine the structural characteristics of the sample under investigation such as the number of graphene layers [3], lattice orientation [4, 5], and edge structure [6]. It also provides information on the level of doping [7], disorder [8], and phonon anharmonicities [9]. The ability of the electron and hole quasiparticles to make phonon-assisted transitions from the valley around $\boldsymbol{K}$ to an equivalent valley around $\boldsymbol{K}'$ yields the prominent 2*D* Raman mode that occurs at $\sim$2700 cm^{-1} for visible irradiation. The 2*D* Raman mode probes the *iTO* phonons around $\boldsymbol{K}$ and shifts to higher phonon frequencies as the incident laser frequency is increased [2]. It is theoretically described, to leading order, by fourth-order perturbation theory [10, 11], i.e., four interaction Hamiltonians: two instances of the electron–radiation interaction Hamiltonians $H_{\mathrm{e-R}}$ for incoming and outgoing photons and two instances of the electron–phonon interaction Hamiltonian $H_{\mathrm{e-ph}}$ (see Fig. 2). This constitutes second-order Raman scattering since the *G* Raman mode that probes the $\boldsymbol{q}\sim 0$ with $\omega_G \sim 1600\,\mathrm{cm}^{-1}$ phonons is described by third-order, and therefore a lower order of perturbation theory. Inspite of this the 2*D* Raman mode of graphene is of comparable intensity to the *G* mode since the phonon-assisted scattering is simulataneously resonant in both the electron and hole channels for the 2*D* mode [10].

Due to the allotropy between two-dimensional graphene and quasi one-dimensional carbon nanotubes and therefore similarities in their basic physics, Raman investigations [12, 13] of graphene were informed by the extensive literature on the Raman spectroscopy of carbon nanotubes (see Ref. [14] for a review). This led to two *a priori* conjectures for the study of graphene. The first being that the dominant phonon wavevectors $\boldsymbol{q}^*$ probed by the 2*D* mode were fixed regardless of the polarization of incoming and outgoing light. The second conjecture was that that the dominant phonon-assisted transitions were restricted along the high symmetry $\boldsymbol{K}-\boldsymbol{M}-\boldsymbol{K}'$ line. These transitions were further distinguished into two types, "inner" [11, 13, 15, 16] and "outer" [3, 12, 15] depending on whether they connected the closer or further edges, respectively, of the equi-excitation energy contours along the $\boldsymbol{K}-\boldsymbol{M}-\boldsymbol{K}'$ line (see Fig. 1).

The two-dimensional nature of graphene warrants a closer look at the two conjectures. Even at first glance, the restriction of the two-dimensional phase space to a single dimensional is liable to miss the effects of quantum mechanical interference [13, 17]. The one-dimensional bands, that are also often considered linear, fail to capture the electron–hole asymmetry of the electronic bands, besides

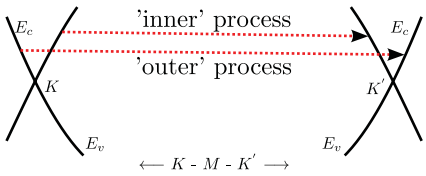

Figure 1 (online color at: www.pss-b.com) The "inner" and "outer" dominant phonon-assisted transitions implicated by the 2*D* Raman mode of graphene.

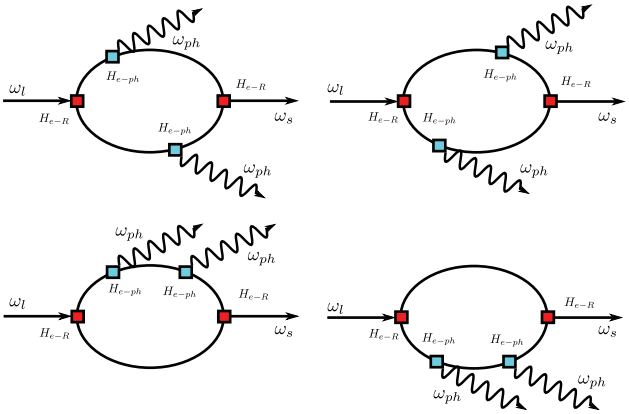

Figure 2 (online color at: www.pss-b.com) The leading Feynman diagrams that contribute to the transition matrix $\mathcal{T}_{fi}(\boldsymbol{q})$ of the 2*D* mode in graphene. $H_{\text{e–R}}$ is the vertex corresponding to electron–radiation interaction Hamiltonian and $H_{\text{e–ph}}$ is the vertex corresponding to the electron–phonon interaction Hamiltonian. ω_{l} and ω_{s} are the incident and scattered photons, repectively, while ω_{ph} is the induced phonon. The upper (lower) branch of each diagram describes the electron (hole) channel.

the trigonal warpings of both the electronic and phonon bands that become prominent at the visible range of laser frequencies [18–20]. Lastly, a simplification is made regarding the wavevector dependence of both the optical and electron–phonon interaction matrix elements: both are taken to be constant across the entire Brillouin zone (BZ). This simplification is emplaced primarily because analytical expressions for the optical matrix elements [21] and the electron–phonon matrix elements [22] are rather cumbersome. The neglect of the opical matrix elements, for instance, precludes the study of the polarization dependence of the 2*D* Raman mode.

In this article we calculate the dominant phonon wavevectors $\boldsymbol{q}^*$ and the associated dominant phonon-assisted electronic transitions probed by the 2*D* Raman mode of graphene for different polarization:analyzer combinations. We explicitly include the full two-dimensional electronic bands and *iTO* phonon branch around $\boldsymbol{K}$ as well as the variation of the optical and electron–phonon matrix elements, all obtained from *ab initio* calculations in a full two-dimensionl integration of the transition matrix.

2 Methodology The two-dimensional electronic eigenfunctions and the optical matrix elements around $\boldsymbol{K}$ were computed using density functional theory (DFT) within the local density approximation (LDA). The two-dimensional electron–phonon matrix elements corresponding to the *iTO* phonon branch around $\boldsymbol{K}$ were calculated using density functional perturbation theory (DFPT) [23]. All calculations were performed using the Quantum ESPRESSO (QE) [24] suite using the established recipe of Ref [9]. For the eigenenergies we used two-dimensional, *GW*-derived electronic bands [25] fit to a third-nearest neighbor tight-binding description [18], and a fit proposed by Ref. [19] for the *iTO* phonon dispersion around $\boldsymbol{K}$. The transition matrix $\mathcal{T}_{fi}(\boldsymbol{q})$ of the 2*D* mode in graphene, corresponding to the leading terms from fourth-order perturbation theory (see the Feynman diagrams of Fig. 2) was evaluated with a single broadening parameter $\gamma = 0.05$ eV [10, 11] and a full two-dimensional integration over the graphene BZ. The dominant phonon-assisted electronic transitions connecting the initial $\boldsymbol{k}_i^*$ and final $\boldsymbol{k}_f^*$ electron wavevectors were determined from the arguments of $\text{Max}[|\mathcal{T}_{fi}(\boldsymbol{k}_i, \boldsymbol{q})|^2]$ and the relation expressing quasi-momentum conservation during the phonon-assisted scattering of the electron and hole quasiparticles ($\boldsymbol{k}_i^* = \boldsymbol{k}_f^* + \boldsymbol{q}^*$).

3 Results and discussion In Fig. 3a–c we show the dominant phonon wavectors $\boldsymbol{q}^*$ for three distinct polarizer:-analyzer combination *x*: *x*, *y*: *y*, and *x*: *y*, repectively. The *x* direction corresponds to the zigzag direction while *y* corresponds to the armchair direction of the graphene lattice. The $\boldsymbol{q}^*$ were extracted from the full two-dimensional integration of the Raman transition matrix involving all the Feynman diagrams of Fig. 2. We clearly see that the $\boldsymbol{q}^*$ are highly anisotropic, not fixed and do not, in general, lie along the $\boldsymbol{K} - \boldsymbol{M} - \boldsymbol{K}'$ line. Instead, they rotate with the direction of the polarizer and span the entire angular extent around the $\boldsymbol{K}$ point. This disproves the first conjecture that $\boldsymbol{q}^*$ are restricted along the $\boldsymbol{K} - \boldsymbol{M} - \boldsymbol{K}'$ line and are independent of the polarization condition. The inferred dominant phonon-assisted transitions connect $\boldsymbol{k}_i^*$ and $\boldsymbol{k}_f^*$ where the product of the optical absorption and emission matrix elements is strongest and lie nominally along the $\boldsymbol{K} - \boldsymbol{M} - \boldsymbol{K}'$ line (see Fig. 4a, b, and c, respectively). Nevertheless crucially, they show a small but significant component along the $\boldsymbol{K} - \boldsymbol{\Gamma}$ line

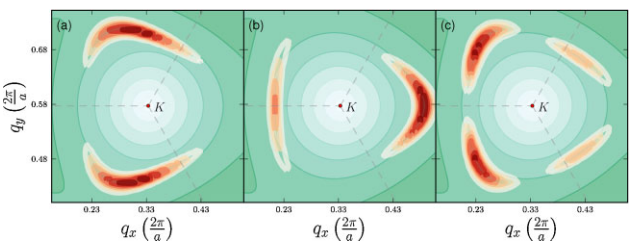

Figure 3 (online color at: www.pss-b.com) The dominant phonon wavevectors $\boldsymbol{q}^*$ (in red-orange) corresponding to polarizer:analyzer orientations: (a) *x*:*x*, (b) *y*:*y*, and (c) *x*:*y*. The underlying green-hued contours depict the *iTO* phonon dispersion of Ref. [19] around $\boldsymbol{K}$.

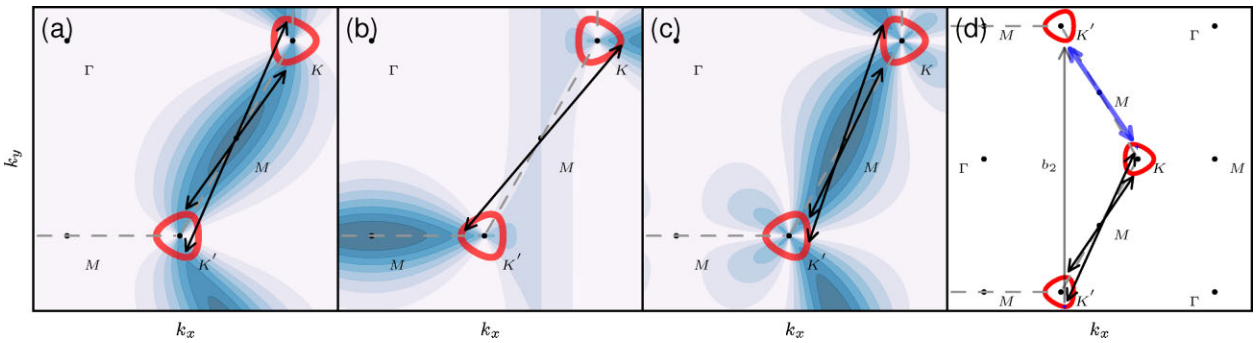

Figure 4 (online color at: www.pss-b.com) The dominant electronic transitions (black double-sided arrows) contributing to the 2*D* mode connect the equi-excitation energy contours (in red) for $E_L = 2.33$ eV around inequivalent $\boldsymbol{K}$ points. (a) *x*:*x*, (b) *y*:*y*, and (c) *x*:*y* (*x*: zigzag, *y*: armchair orientation of graphene). The two dominant transitions shown for (a) *x*:*x* and (c) *x*:*y* contribute equally to the 2*D* mode. The underlying white-blue contour plot in (a)–(c) is the product of the optical absorption and emission matrix elements corresponding to the polarizer and analyzer orientations as a function of the electronic wave vector at which the transition occurs. (d) For the *x*:*x* case, on adding a reciprocal lattice vector $\boldsymbol{b}_2$ to $\boldsymbol{k}_i^*$, from the seemingly "outer" dominant transition (black double-sided arrow) an equivalent "inner" electronic transition (blue double-sided arrow) is obtained.

that sensitively determines the angular location of $\boldsymbol{q}^*$. However, the dominant phonon-assisted electronic transitions are not affected by the structure of the electron–phonon matrix elements.

Already, the notion of "inner" and "outer" processes occuring along the high symmetry $\boldsymbol{K}-\boldsymbol{M}-\boldsymbol{K}'$ is appearing questionable since the dominant phonon-assisted transitions show a component along the $\boldsymbol{K}-\boldsymbol{\Gamma}$ direction. Further, we observe that by adding a reciprocal lattice vector $\boldsymbol{b}_2$ to $\boldsymbol{k}_i^*$, the dominant phonon-assisted electronic transition changes from being seemingly "outer" (the black double sided arrow connecting the cross hairs located on the equi-excitation energy contours) to an entirely equivalent "inner" transition (the heavy blue double sided arrow) (see Fig. 4d). In general, each apparently "inner" process posesses an entirely equivalent "outer" process, thus undermining the distinction between them. Thus, we are able to dismiss the notion of "inner" and "outer" processes. They neither lie along the high symmetry $\boldsymbol{K}-\boldsymbol{M}-\boldsymbol{K}'$ line, nor are they distinct, thereby disproving the second conjecture regarding distinct "inner" and "outer" processes. A further comment regarding the validity of inferring the dominant phonon-assisted transitions from a Raman experiment is in order. Strictly speaking, the electronic wavevectors $\boldsymbol{k}$ are not observables of the Raman experiment and therefore inaccessible as they mutually interfere in the expression for $\mathcal{T}_{fi}(\boldsymbol{q})$ as intermediate states [26]. Physically, the Raman experiment only accesses the $\omega(\boldsymbol{q}^*)$, where $\boldsymbol{q}^*$ change dramatically with the polarizer:analyzer condition. In the absence of a symmmetry breaking potential, the anisotropy and rotation of $\boldsymbol{q}^*$ notwithstanding, $\boldsymbol{q}^*$ run parallel to the phonon energy contours (see Fig. 3a–c) yielding the 2*D* mode at the same frequency and profile.

The foregoing discussion points to the importance of determining the polarizer:analyzer orientation with respect to the lattice orientation of graphene in order to set the $\boldsymbol{q}^*$ distribution. In Fig. 5 we show the angular $\theta_{\boldsymbol{q}^*}$ and radial dependence $r_{\boldsymbol{q}^*}$ of $\boldsymbol{q}^*$ probed by the 2*D* mode with the polarizer and analyzer orientations set parallel to each other. This suggests that polarized Raman measurements of the 2*D* mode on graphene with predetermined lattice orientation, while sweeping the laser energy, provide a means of determining the complete two-dimensional *iTO* dispersion around $\boldsymbol{K}$. As an aside we mention that the orientation of the graphene lattice (e.g., zigzag or armchair) is easily determined via Raman spectroscopy [4, 5]. Procedurally, a comprehensive *phonon mapping* experiment may be performed as follows, first, determine the lattice orientation of graphene from the procedure given in Ref. [4, 5]. Next, align

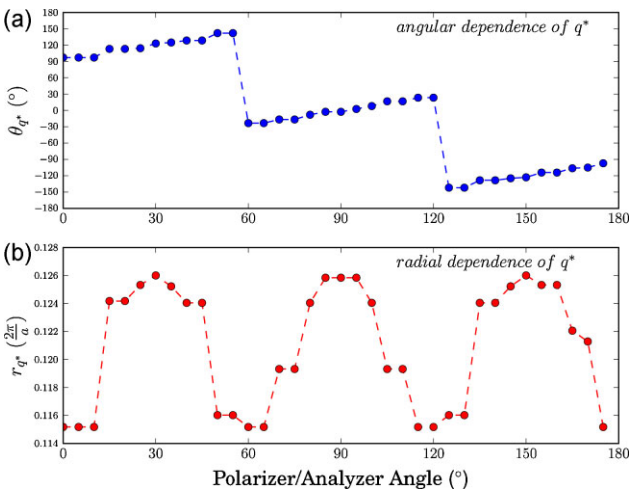

Figure 5 (online color at: www.pss-b.com) (a) The angular variation $\theta_{\boldsymbol{q}^*} = \text{atan2}\left(\frac{q_y^*-K_{1y}}{q_x^*-K_{1x}}\right)$ of $\boldsymbol{q}^*$ around $\boldsymbol{K}_1 \equiv \left(\frac{1}{3}, \frac{1}{\sqrt{3}}\right)\left(\frac{2\pi}{a}\right)$ with polarizer = analyzer orientation relative to the graphene lattice. (b) The radial dependence $r_{\boldsymbol{q}^*} = \sqrt{(q_x^*-K_{1x})^2+(q_y^*-K_{1y})^2}$ of $\boldsymbol{q}^*$ around $\boldsymbol{K}_1$. The zero of the polarizer orientation corresponds to the zigzag direction.

the polarizer and analyzer parallel to each other and set their zero position along the zigzag direction of graphene. Finally, measure the position of the 2*D* mode for every polarizer/analyzer orientation with θ_{q^*} and r_{q^*} given by Fig. 5a and b, repectively. Increasing the laser frequency shall give access to the outer reaches of the *iTO* phonon dispersion around $\boldsymbol{K}$.

4 Summary We have calculated the dominant phonon wavectors $\boldsymbol{q}^*$ and the associated dominant phonon-assisted electronic transitions for the 2*D* Raman mode of graphene. We explicitly included the two-dimensional electronic bands and the *iTO* phonon branch around $\boldsymbol{q}^*$ besides the $\boldsymbol{k}$ and $\boldsymbol{q}$ dependence of the optical and electron–phonon matrix elements from *ab initio* calculations in a full two-dimensional integration for the transition matrix. We found that $\boldsymbol{q}^*$ display a highly anisotropic structure and rotate with the polarizer:analyzer orientation with respect to the crystallographic orientation of graphene, probing the entire angular dependence of the phonons about $\boldsymbol{K}$. The associated dominant electronic transitions are neither fixed, nor parallel to the $\boldsymbol{K}-\boldsymbol{M}-\boldsymbol{K}'$ direction. Instead, a small but significant contribution of the $\boldsymbol{K}-\boldsymbol{\Gamma}$ direction is discerned, connecting regions where the product of the optical absorption and emission matrix elements for given polarizer:analyzer orientation is strongest. Each apparently ''inner'' process can be transformed by translation of $\boldsymbol{k}_i^*$ with a reciprocal lattice vector into an entirely equivalent ''outer'' process and *vice versa*. Thus, we are able to completely dismiss the concept of ''inner'' and ''outer'' processes and rather commend the use of the characteristic $\boldsymbol{q}^*$ as the illuminating notion instead. Our findings are expected to be crucial for the correct interpretation of Raman 2*D* and the theoretically closely-related, defect-activated *D* mode measurements on both pristine and strained graphene [27].

Acknowledgements This work was supported by the MIT Institute of Soldier Nanotechnologies (ISN) and the European Research Council (ERC) under grant number 210642-OptNano.

References

[1] K. S. Novoselov, A. K. Geim, S. V. Morozov, D. Jiang, Y. Zhang, S. V. Dubonos, I. V. Grigorieva, and A. A. Firsov, Science **306**(5696), 666–669 (2004).
[2] S. Reich and C. Thomsen, Philos. Trans. R. Soc. A **362**(1824), 2271–2288 (2004).
[3] A. C. Ferrari, J. C. Meyer, V. Scardaci, C. Casiraghi, M. Lazzeri, F. Mauri, S. Piscanec, D. Jiang, K. S. Novoselov, S. Roth, and A. K. Geim, Phys. Rev. Lett. **97**(18), 187401 (2006).
[4] T. M. G. Mohiuddin, A. Lombardo, R. R. Nair, A. Bonetti, G. Savini, R. Jalil, N. Bonini, D. M. Basko, C. Galiotis, N. Marzari, K. S. Novoselov, A. K. Geim, and A. C. Ferrari, Phys. Rev. B **79**(20), 205433 (2009).
[5] M. Huang, H. Yan, C. Chen, D. Song, T. F. Heinz, and J. Hone, Proc. Natl. Acad. Sci. **106**(18), 7304–7308 (2009).
[6] L. G. Cançado, M. A. Pimenta, B. R. A. Neves, M. S. S. Dantas, and A. Jorio, Phys. Rev. Lett. **93**(24), 247401 (2004).
[7] S. Pisana, M. Lazzeri, C. Casiraghi, K. S. Novoselov, A. K. Geim, A. C. Ferrari, and F. Mauri, Nature Mater. **6**(3), 198–201 (2007).
[8] A. C. Ferrari, Solid State Commun. **143**, 47–57 (2007).
[9] N. Bonini, M. Lazzeri, N. Marzari, and F. Mauri, Phys. Rev. Lett. **99**(17), 176802 (2007).
[10] R. Narula, Resonant Raman Scattering in Graphene, PhD thesis, Massachusetts Institute of Technology (2011).
[11] P. Venezuela, M. Lazzeri, and F. Mauri, Phys. Rev. B **84**(3), 035433 (2011).
[12] R. Saito, A. Jorio, A. G. Souza Filho, G. Dresselhaus, M. S. Dresselhaus, and M. A. Pimenta, Phys. Rev. Lett. **88**(2), 027401 (2001).
[13] J. Maultzsch, S. Reich, and C. Thomsen, Phys. Rev. B **70**(15), 155403 (2004).
[14] S. Reich, C. Thomsen, and J. Maultzsch, Carbon Nanotubes (Wiley-VCH, Berlin, 2004).
[15] M. Mohr, J. Maultzsch, and C. Thomsen, Phys. Rev. B **82**(20), 201409 (2010).
[16] D. Yoon, Y. W. Son, and H. Cheong, Phys. Rev. Lett. **106**(15), 155502 (2011).
[17] R. Narula and S. Reich, Phys. Rev. B **78**(16), 165422 (2008).
[18] S. Reich, J. Maultzsch, C. Thomsen, and P. Ordejón, Phys. Rev. B **66**(3), 035412 (2002).
[19] A. Gruneis, J. Serrano, A. Bosak, M. Lazzeri, S. L. Molodtsov, L. Wirtz, C. Attaccalite, M. Krisch, A. Rubio, F. Mauri, and T. Pichler, Phys. Rev. B **80**(8), 085423 (2009).
[20] R. Narula, R. Panknin, and S. Reich, Phys. Rev. B **82**(4), 045418 (2010).
[21] A. Gruneis, R. Saito, G. G. Samsonidze, T. Kimura, M. A. Pimenta, A. Jorio, A. G. S. Filho, G. Dresselhaus, and M. S. Dresselhaus, Phys. Rev. B **67**(16), 165402 (2003).
[22] L. Pietronero, S. Strässler, H. R. Zeller, and M. J. Rice, Phys. Rev. B **22**(2), 904–910 (1980).
[23] S. Baroni, S. de Gironcoli, A. Dal Corso, and P. Giannozzi, Rev. Mod. Phys. **73**(2), 515–562 (2001).
[24] P. Giannozzi, S. Baroni, N. Bonini, M. Calandra, R. Car, C. Cavazzoni, D. Ceresoli, G. L. Chiarotti, M. Cococcioni, I. Dabo, A. D. Corso, S. de Gironcoli, S. Fabris, G. Fratesi, R. Gebauer, U. Gerstmann, C. Gougoussis, A. Kokalj, M. Lazzeri, L. Martin-Samos, N. Marzari, F. Mauri, R. Mazzarello, S. Paolini, A. Pasquarello, L. Paulatto, C. Sbraccia, S. Scandolo, G. Sclauzero, A. P. Seitsonen, A. Smogunov, P. Umari, and R. M. Wentzcovitch, J. Phys.: Condens. Matter **21**(39), 395502 (2009).
[25] A. Gruneis, C. Attaccalite, L. Wirtz, H. Shiozawa, R. Saito, T. Pichler, and A. Rubio, Phys. Rev. B **78**(20), 205425 (2008).
[26] C. Cohen-Tannoudji, J. Dupont-Roc, and G. Grynberg, Atom–Phonon Interactions: Basic Processes and Applications (John Wiley & Sons, New York, 1992).
[27] M. Huang, H. Yan, T. F. Heinz, and J. Hone, Nano Lett. **10**(10), 4074–4079 (2010).

